Available online at www.sciencedirect.com
ScienceDirect
www.elsevier.com/locate/brainres
Brain Research

Research Report

Modeling the evolving oscillatory dynamics of the rat locus coeruleus through early infancy

Mainak Patel[a,*], Badal Joshi[b]

[a]Department of Mathematics, College of William and Mary, United States
[b]Department of Mathematics, California State University, San Marcos, United States

ARTICLE INFO

Article history:
Accepted 23 May 2015
Available online 4 June 2015

Keywords:
Locus coeruleus
Sleep–wake
Gap junction
Inhibition
Infant development
Network oscillation
Neuronal synchrony
Neuronal network
Network structure and function
Neuron model

ABSTRACT

The mammalian locus coeruleus (LC) is a brainstem structure that displays extensive interconnections with numerous brain regions, and in particular plays a prominent role in the regulation of sleep and arousal. Postnatal LC development is known to drastically alter sleep–wake switching behavior through early infancy, and, in rats, exerts its most significant influence from about postnatal day 8 to postnatal day 21 (P8–P21). Physiologically, several dramatic changes are seen in LC functionality through this time period. Prior to P8, LC neurons are extensively coupled via electrical gap junctions and chemical synapses, and the entire LC network exhibits synchronized ~0.3 Hz subthreshold oscillations and spiking. From P8 to P21, the network oscillation frequency rises up to ~3 Hz (at P21) while the amplitude of the network oscillation decreases. Beyond P21, synchronized network oscillations vanish and gap junction coupling is sparse or nonexistent. In this work, we develop a large-scale, biophysically realistic model of the rat LC and we use this model to examine the changing physiology of the LC through the pivotal P8–P21 developmental period. We find that progressive gap junction pruning is sufficient to account for all of the physiological changes observed from P8 to P21.

© 2015 Elsevier B.V. All rights reserved.

1. Introduction

The locus coeruleus (LC), a small but important neuronal population within the brainstem, is known to diffusely innervate many key brainstem structures involved in sleep–wake regulation and plays a pivotal role in mammalian sleep and arousal behavior (Andrew Gall et al., 2009), particularly through early postnatal development. Prior experiments in rats have provided several tantalizing clues as to the impact of the LC on the development of sleep–wake cycling from infancy into adulthood. In the early postnatal period (up to postnatal day 8, or P8), rats randomly switch between the sleeping and waking states, spending an exponentially distributed amount of time in a given state prior to a switch. While the mean time spent in each state increases from P2 to P8, the length of sleep or wake bouts remains exponentially distributed (Halász et al., 2004; Lo et al., 2004, 2002; Blumberg et al., 2005; Andrew Gall et al., 2009; Karlsson et al., 2005, 2004; Kleitman and Engelmann, 1953).

Behavioral sleep and wake bouts are correlated with the activity of 'sleep-active' and 'wake-active' populations within the brain that are likely to reciprocally inhibit each other. During a sleep bout, 'sleep-active' neurons fire and

*Corresponding author: Tel.: +1 7572214628.
E-mail address: mjpatel@wm.edu (M. Patel).

http://dx.doi.org/10.1016/j.brainres.2015.05.033
0006-8993/© 2015 Elsevier B.V. All rights reserved.

'wake-active' neurons are quiet, while during a wake bout, 'wake-active' neurons fire and 'sleep-active' neurons are silent. Numerous 'sleep-active' and 'wake-active' populations have been found. Examples of sleep-active populations include the ventrolateral preoptic area (VLPO), medullary inhibitory area (MIA), nucleus pontis oralis (PO), and subcoeruleus (subLC). Wake-active populations are divided into two branches: (1) the thalamic branch (e.g., laterodorsal tegmentum or LDT, pedunculopontine tegmentum or PPT) and (2) the hypothalamic branch (e.g., dorsal raphe nuclei or DR, tuberomamillary nucleus or TMN) (Blumberg et al., 2005; Karlsson et al., 2005; Schwartz and Roth, 2008). In prior work, we investigate switching between neonatal sleep-active and wake-active populations in a simplified two-neuron model (Patel and Joshi, 2014), and we are currently extending these results to mutually inhibitory *populations* of sleep-active and wake-active cells.

From P8 to P21, mean sleep and wake bout lengths continue to increase, and sleep bout times remain exponentially distributed; wake bouts, however, undergo a dramatic *qualitative* change – wake bout lengths gradually develop a heavy-tailed, power law-like distribution (Blumberg et al., 2005). Experimental evidence strongly establishes that the LC is responsible for this qualitative shift in the nature of wake bout times (Berridge et al., 2012; Saper et al., 2001; Takahashi et al., 2010; Aston-Jones and Bloom, 1981; Andrew Gall et al., 2009).

Interestingly, and in step with the remarkable changes in sleep–wake behavior observed through early rat infancy, the rat LC simultaneously exhibits drastic shifts in its physiology and dynamics. In infant rats, experiments have shown that LC neurons display synchronized subthreshold membrane potential oscillations (and synchronized spiking), a tendency which diminishes and finally disappears as the animal ages. Prior to P8, synchronized oscillations have relatively large amplitude (up to 15 mV) and low frequency (~0.3 Hz); the amplitude of synchronized subthreshold oscillations decreases while the frequency increases (up to ~3 Hz) from P8 to P21, after which LC-wide synchrony is rarely observed. Evidence suggests that synchrony across LC neurons in infants may be due to extensive (but weak) electrical coupling via dendro-dendritic gap junctions throughout the entire LC network, while by P21 gap junction connectivity is considerably reduced and insufficient to synchronize LC neurons under normal physiological conditions (Christie, 1997; Coyle and Molliver, 1977; Christie et al., 1989; Travagli et al., 1995; Christie and Jelinek, 1993; Williams and Marshall, 1987; Ishimatsu and Williams, 1996; Groves and Wilson, 1980).

The intriguing concordance between shifting sleep–wake behavior and changing LC physiology during the P8–P21 period suggests that the observed changes in LC functioning may underlie the ability of the LC to modify and influence the physiological behavior of infant sleep-active and wake-active populations. In order to understand the interaction of the LC with brainstem sleep–wake circuitry, a crucial first step is to understand the physiological mechanisms responsible for the evolution of LC dynamics through the early postnatal period.

The rat LC contains ~1500 noradrenergic neurons, and in the infant the probability of electrical coupling between a pair of LC cells is ~0.4. Electrical coupling has been shown to be weak – current injection into cell 1 of a pair of electrically coupled LC cells sufficient to cause a 100 mV depolarization produces only a ~2 mV change in the membrane potential of cell 2. Moreover, if current is injected into cell 1, the time constant of the membrane potential response of cell 1 is ~10 to 20 ms, while the time constant of the potential change in cell 2 (in response to electrical input from cell 1) is ~100 to 300 ms. This suggests that electrical coupling occurs in distal dendrites, and it is important to note that 2 ms action potentials are too fast to be transmitted via the slow gap junctions (Christie, 1997; Christie et al., 1989; Travagli et al., 1995). Synaptic coupling among LC neurons is both excitatory and inhibitory, with coupling properties changing through development. Inhibitory synaptic coupling persists throughout the lifespan of the LC and is mediated via α_2 adrenergic receptors (both presynaptic and postsynaptic), which induce hyperpolarization via opening of K^+ channels, leading to long ~1 to 2 s potential changes (Christie, 1997; Egan et al., 1983; Groves and Wilson, 1980; Ennis and Aston-Jones, 1986). Excitatory synaptic coupling among LC neurons is mediated via α_1 adrenergic receptors transiently in early infancy, while from ~P8 to P21 α_1 receptors vanish and excitatory coupling among LC neurons disappears (Williams and Marshall, 1987). Additionally, evidence indicates that individual LC neurons exhibit intrinsic Ca^{2+} currents and Ca^{2+}-dependent K^+ currents, which may contribute to the subthreshold membrane potential oscillations seen in individual LC neurons, though evidence suggests that synaptic inhibition is sufficient for generating oscillations (Coyle and Molliver, 1977; Ennis and Aston-Jones, 1986). Finally, LC neurons receive synaptic excitatory inputs which induce ~100 ms potential changes from outside the LC network (Cherubini and North, 1988).

In this work, we construct a large-scale computational network model of the rat LC in order to examine the emergence of LC-wide synchrony and subthreshold oscillations, as well as the increase in oscillation frequency and decrease in oscillation amplitude that occurs as the LC ages from P8 to P21, and finally the disappearance of global oscillations and synchrony beyond P21. In the neonatal LC (in which LC neurons are extensively coupled via gap junctions), the network oscillation frequency is ~0.3 Hz (Christie, 1997), corresponding to a period of ~3 s, which is consistent with the long time course of synaptic inhibition induced through α_2 adrenergic receptors. Furthermore, data suggest that intrinsic mechanisms are not essential in generating the post-activation inhibition observed in LC neurons, and that synaptic mechanisms are sufficient (Ennis and Aston-Jones, 1986). Hence, we employ a scaled-down, biophysical model of the neonatal LC consisting of 120 integrate-and-fire neurons coupled via weak dendritic gap junctions and inhibitory α_2 receptors (since spikes are too fast to be transmitted via slow dendritic gap junctions, explicit modeling of the spiking mechanism is unnecessary). We show that our model is capable of reproducing the ~0.3 Hz LC-wide synchronized oscillations observed in the neonatal rat LC, and that progressive gap junction pruning within our model can account for the increasing oscillation frequency and declining oscillation amplitude seen during the P8–P21 period, as well as the disappearance of network coherence after P21. Furthermore,

we examine the dependence of the behavior of our LC model on various network parameters.

2. Results

Our model of the rat neonatal LC consists of 120 neurons governed by integrate-and-fire dynamics with all-to-all gap junction coupling. Since the neonatal rat LC contains 1500 neurons with cells coupled to each other via slow dendro-dendritic gap junctions with a coupling probability of ~0.4 (Christie, 1997), we set a high electrical coupling probability in our network to compensate for the reduced scale of our model. We simulate the slow dendro-dendritic gap junctions of the rat LC within our model by modifying the input voltage to a neuron from a gap junction – if neuron i within the model is electrically coupled to neuron j, then the input voltage to neuron i from neuron j at time t is given by the membrane potential of neuron j averaged over the past 50 ms. We find that this computationally efficient scheme for simulating slow dendro-dendritic gap junctions yields similar results to explicitly rendering a separate dendritic compartment. Neurons within our model are also chemically coupled through strong inhibitory synapses, with a random inhibitory coupling probability of 0.5 from any one cell to another. Synaptic inhibition is slow, and each neuron within the model is coupled to itself, since the α_2 adrenergic receptors mediating synaptic inhibition within the rat LC are present both presynaptically and postsynaptically (Christie, 1997; Egan et al., 1983; Groves and Wilson, 1980; Ennis and Aston-Jones, 1986). Since experiments indicate that intrinsic Ca and Ca-dependent K currents are not necessary to produce the post-activation inhibition in LC neurons that gives rise to oscillations (Ennis and Aston-Jones, 1986), we omit these currents from our model. Finally, all neurons within our system receive an excitatory drive constructed independently for each cell as a Poisson process of incoming spikes from outside the LC, in accordance with the experimentally observed dynamics of external excitation impinging upon the neonatal rat LC (Cherubini and North, 1988). We measure the oscillatory behavior of our network by computing the Fourier transform of the simulated local field potential (LFP), which we compute as the average membrane potential of all neurons within the network. A schematic of our model is shown in Fig. 1. Details of the model, and experimental justification of network parameter choices, are given in the *Methods*.

2.1. *Neonatal LC dynamics (up to P8)*

We begin by assessing the necessity of both gap junctions and synaptic inhibition for generating synchronized oscillations within our neonatal LC model. As shown in Fig. 2A, synaptic inhibition alone (without electrical coupling among cells), is unable to either synchronize network cells or yield oscillatory behavior in a single neuron (the lack of synchrony can be seen in the spike raster in the left panel of Fig. 2A and the Fourier transform of the network's LFP in the right panel, while the lack of oscillatory behavior in a single neuron is evident from the plot of a sample neuron's membrane

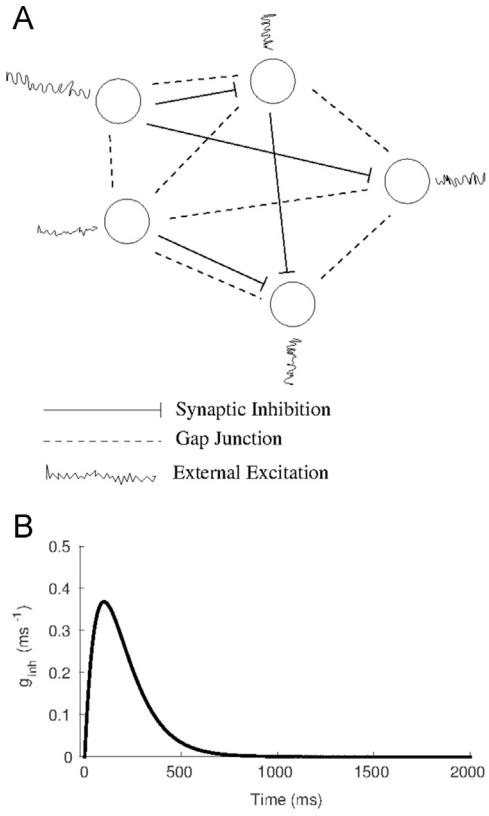

Fig. 1 – (A) The LC model network consists of 120 integrate and fire neurons, each of which receives an independent, noisy excitatory drive. Neurons are electrically coupled via slow gap junctions and chemically coupled via slow inhibitory synapses. Electrical coupling is all-to-all, while the probability of an inhibitory chemical synapse from one neuron to another is set to 0.5. (B) Postsynaptic inhibitory conductance change elicited by a presynaptic spike.

potential in the middle panel). Without gap junctions, the noisy excitatory drive yields random, sporadic spiking, and due to the extensive synaptic connectivity of the network, at any given moment in time each neuron receives a constant mean level of inhibition corresponding to the steady-state firing rate of the network. Fig. 2B shows network behavior in the presence of gap junction coupling but with synaptic inhibition removed from the model – gap junctions suffice to synchronize neuronal spiking, but cannot generate a network oscillation. As a consequence of electrical coupling, production of one or a few spikes results in a synchronous burst of network spikes, and hence network spikes occur in coincident bursts; however, the time between bursts is random, determined by the fluctuations in the noisy excitatory drive impinging upon neurons. The presence of both electrical and chemical coupling, however, yields both network synchrony as well as oscillatory behavior; Fig. 2C (left and middle) shows network-wide synchrony as well as subthreshold oscillations in a sample neuron, with the oscillation frequency given by ~0.4 Hz (as seen in the peak of the LFP power spectrum in the right panel), which is concordant with experiment (Christie, 1997). Gap junctions serve to synchronize neurons across the model LC network, causing neurons

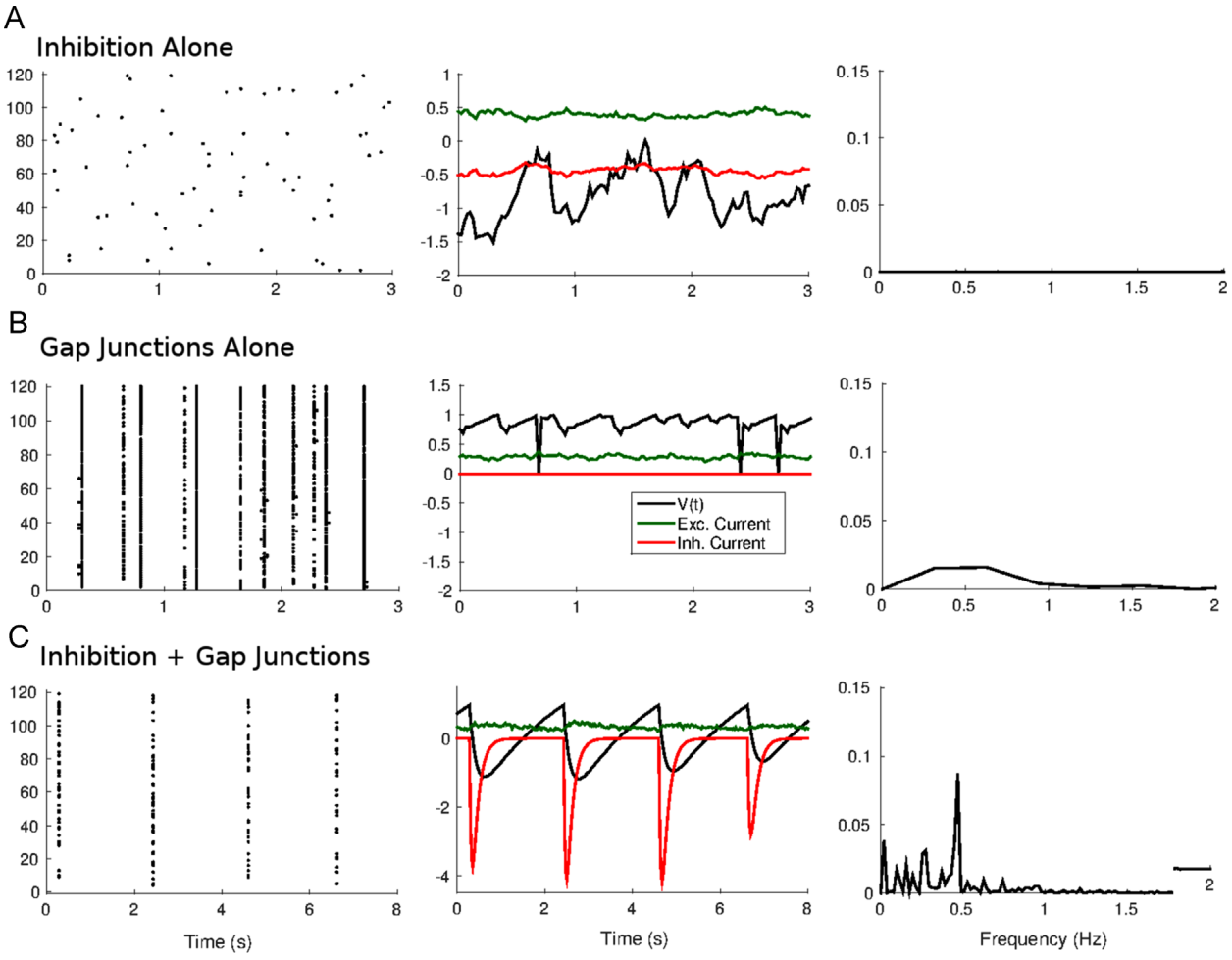

Fig. 2 – Both gap junctions and synaptic inhibition are required to obtain network-wide synchronized 0.4 Hz oscillations and spiking. Spike rasters (*left*), membrane potential of a representative network neuron (*middle*), and power spectrum of the network's local field potential (*right*) are shown in three cases: (A) synaptic inhibition remains intact but all gap junctions are removed; (B) gap junctions remain intact but synaptic inhibition is removed; (C) both gap junctions and synaptic inhibition are present. P[gap junction coupling]=1, while P[inhibitory synaptic coupling]=0.5.

to produce spikes in simultaneous bursts, and each burst of spikes results in the activation of inhibitory synapses throughout the network, yielding network-wide inhibitory suppression and delaying the next burst of spikes with a characteristic temporal scale (the persistence time scale of synaptic inhibition).

If Fig. 3, we show the dependence of the network oscillation on the strength of inhibitory synapses within the network – we show network behavior when the amplitude of the postsynaptic inhibitory conductance change induced by a presynaptic spike is multiplied by 0.5, 0.25, or 0.1. The plots suggest that as the strength of inhibition is decreased, the crispness and strength of network oscillations declines (compare the peak sizes of the power spectra in Fig. 3 with the power spectrum of the standard network in Fig. 2C), while the network oscillation frequency is minimally affected. Accordingly, Fig. 4 shows that the integrated power in the 0.1–4 Hz range of the power spectrum of the network LFP decreases monotonically as the strength of synaptic inhibition within the network is reduced. Thus, we can conclude that the strength of synaptic inhibition within the network determines the amplitude or sharpness of the network oscillation, while having little impact on the network's oscillation frequency.

In contrast, the time course of synaptic inhibition directly determines the oscillation frequency of the network. In Fig. 5, we show spike rasters of the network in the case of varying temporal profiles of synaptic inhibition. Fig. 5A shows the different time courses of synaptic inhibition employed, while Fig. 5B shows spike rasters from the standard network corresponding to the synaptic inhibition profiles depicted in Fig. 5A and 5C shows spike rasters corresponding to each inhibitory profile in the case that gap junctions are permitted instantaneous dynamics (i.e., when the input voltage to neuron i from gap junction-coupled neuron j at time t is given by $v_j(t)$, rather than by $v_j(t)$ averaged over the past 50 ms; this simulates fast somatic gap junctions rather than the slow dendro-dendritic gap junctions observed in the rat LC).

Fig. 5 shows, as expected, that as the time course of synaptic inhibition is shortened, the oscillation frequency of the network rises – gap junction coupling effects synchronous bursts of neuronal spikes, and the time course of synaptic inhibition

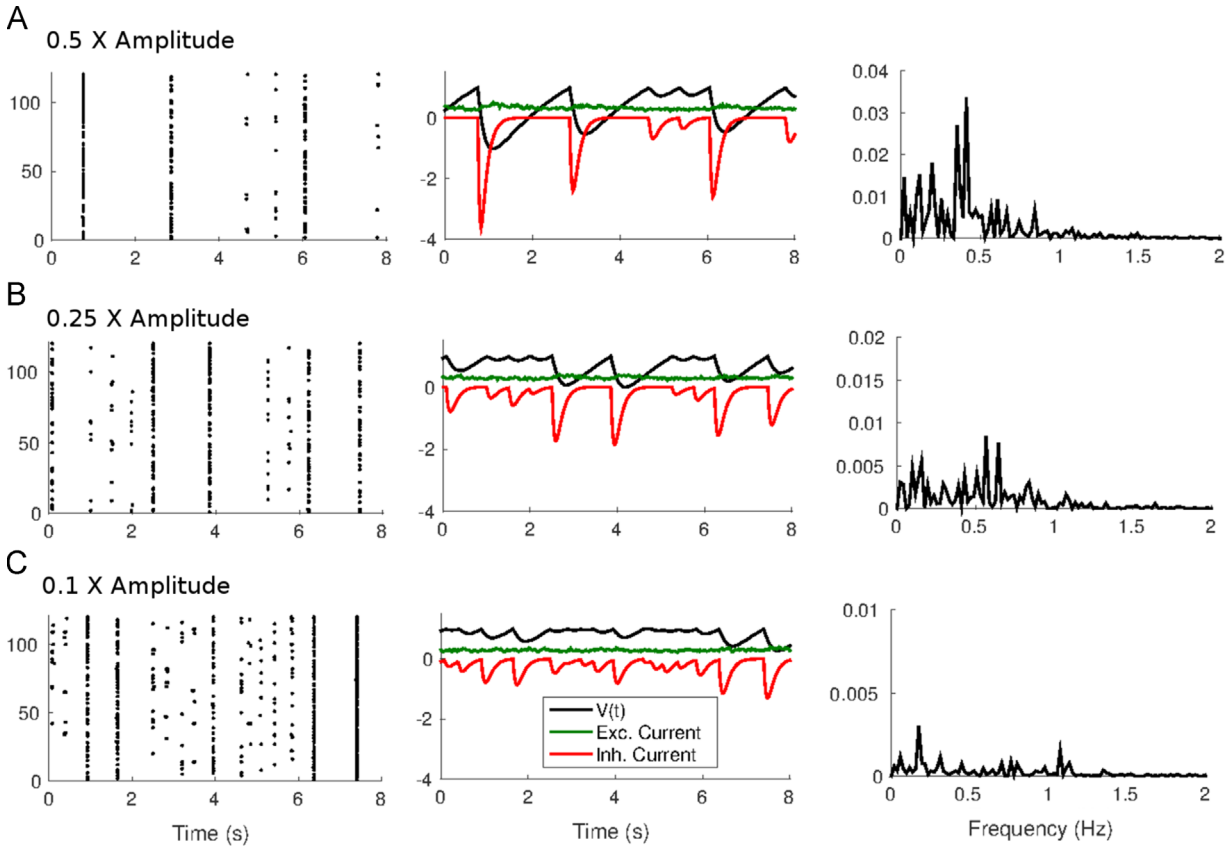

Fig. 3 – Dependence of network-wide oscillations on the amplitude of the postsynaptic inhibitory conductance change elicited by a presynaptic spike. Spike rasters (*left*), membrane potential of a representative network neuron (*middle*), and power spectrum of the network's local field potential (*right*) are shown when the amplitude of synaptic inhibition is set to (A) 0.5, (B) 0.25, or (C) 0.1 times its standard value. P[gap junction coupling]=1, while P[inhibitory synaptic coupling]=0.5.

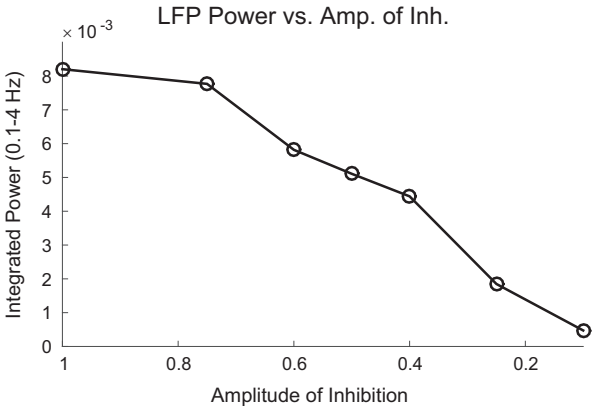

Fig. 4 – Dependence of network-wide oscillations on the amplitude of the postsynaptic inhibitory conductance change elicited by a presynaptic spike. The figure shows integrated power in the 0.1–4 Hz range of the network local field potential's power spectrum as a function of the amplitude of synaptic inhibition (represented as the factor multiplied by the standard value). As inhibitory amplitude decreases, the oscillatory tendency of the network declines. P[gap junction coupling]=1, while P[inhibitory synaptic coupling]=0.5.

determines the temporal length of network quiescence induced by each spike burst, giving rise to synchronous bursts with a characteristic interburst interval. However, Fig. 5B and C shows that the temporal dynamics of electrical coupling play a role in the effectiveness of gap junctions in synchronizing network cells. For a low network oscillation frequency of ~0.3 Hz (i.e., a long time course of synaptic inhibition), either slow or fast gap junctions are able to synchronize neurons and yield network-wide oscillations (left panels). For high network oscillation frequencies of ~2.5–3 Hz (i.e., short inhibitory time courses), gap junctions must enforce network-wide synchrony over a time scale considerably shorter than the temporal length of synaptic inhibition in order for synchronized network oscillations to emerge – slow gap junctions, due to their ~50 ms dynamics, are unable to synchronize cells over such short time scales, and hence cannot give rise to synchronized network oscillations, while fast gap junctions are capable of synchronizing cells over nearly instantaneous time scales, and so can yield a high-frequency network oscillation (middle and right panels).

2.2. *LC dynamics through development (P8–P21)*

From P8 to P21, the oscillation frequency of the rat LC network rises up to ~3 Hz, while the amplitude of the network oscillation declines and gap junctions within the network are progressively pruned and ultimately vanish (Christie, 1997; Coyle and Molliver, 1977; Christie et al., 1989; Travagli et al., 1995; Christie and Jelinek, 1993; Williams and Marshall, 1987; Ishimatsu and Williams, 1996; Groves and

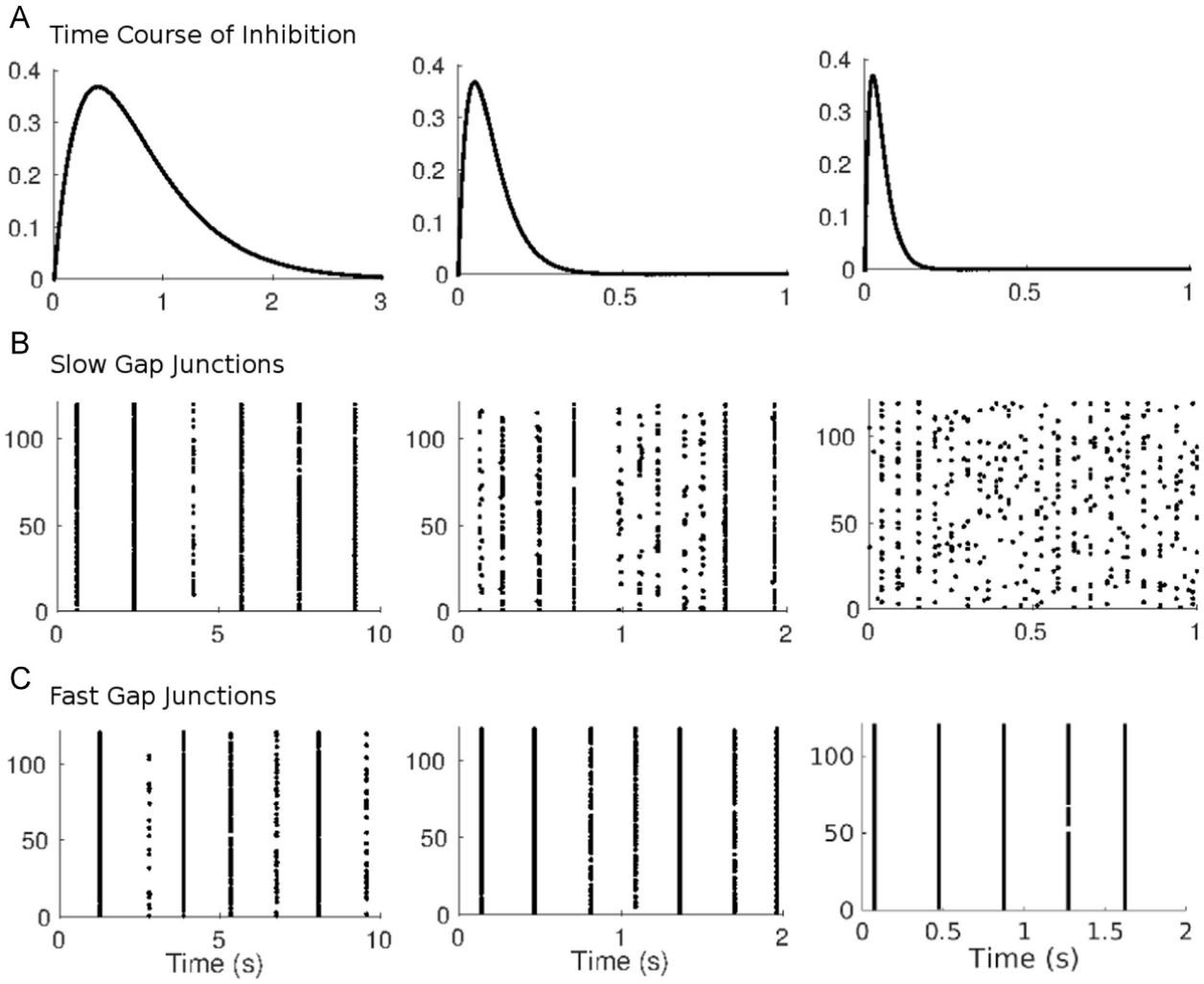

Fig. 5 – The network-wide oscillation frequency is determined by the time course of synaptic inhibition. (A) Time course of the postsynaptic inhibitory conductance change elicited by a presynaptic spike. (B) Spike rasters corresponding to the various inhibitory time courses in the case of normal (slow) gap junctions. (C) Spike rasters corresponding to the various inhibitory time courses in the case of fast (instantaneous) gap junctions. Slow gap junctions are capable of yielding network-wide oscillatory synchrony for low oscillation frequencies (*left column*) but have difficulty synchronizing the network on short oscillatory time scales (*right columns*). Fast gap junctions can yield network-wide oscillatory synchrony for all oscillation time scales. P[gap junction coupling]=1, while P[inhibitory synaptic coupling]=0.5.

Wilson, 1980). Our results above suggest that modifying the temporal profile of synaptic inhibition cannot account for the rising oscillation frequency of the rat LC from P8 to P21, since the rat LC contains slow dendro-dendritic synapses (Christie, 1997; Christie et al., 1989; Travagli et al., 1995), which our results suggest are unable to synchronize LC cells on short enough time scales to allow for a network oscillation period of less than ~500 ms. However, we now show that random gap junction pruning is able to account for the experimentally observed changes in LC behavior in the P8–P21 period.

Whether neuron *i* is coupled to neuron *j* is determined by a randomly generated number between 0 and 1 – if this random number is less than the gap junction coupling probability of the network, neurons *i* and *j* are coupled, otherwise they are not. Reductions in the gap junction coupling probability of the network are effected by decreasing the gap junction coupling probability of the network while keeping the same random seed for the simulation; this causes the same random numbers to be generated, with the only difference being a decrease in the threshold required for two neurons to lack electrical coupling. Once the (fixed) random number generated for neurons *i* and *j* is greater than this threshold, the gap junction between neurons *i* and *j* is eliminated. Hence, this scheme corresponds to reductions in the gap junction probability of the network yielding progressive elimination of gap junctions within the network while maintaining the remaining network architecture (as would be expected of progressive gap junction pruning within the rat LC).

In Fig. 6, we depict network behavior for various values of the gap junction coupling probability of the network; left panels show the network spike raster, middle panels plot the membrane potential of a representative network cell, and right panels show the power spectrum of the network LFP. A coupling probability of 0.8 (as opposed to the neonatal all-to-all coupling) causes the frequency of the network oscillation to rise to ~0.7 Hz (from the

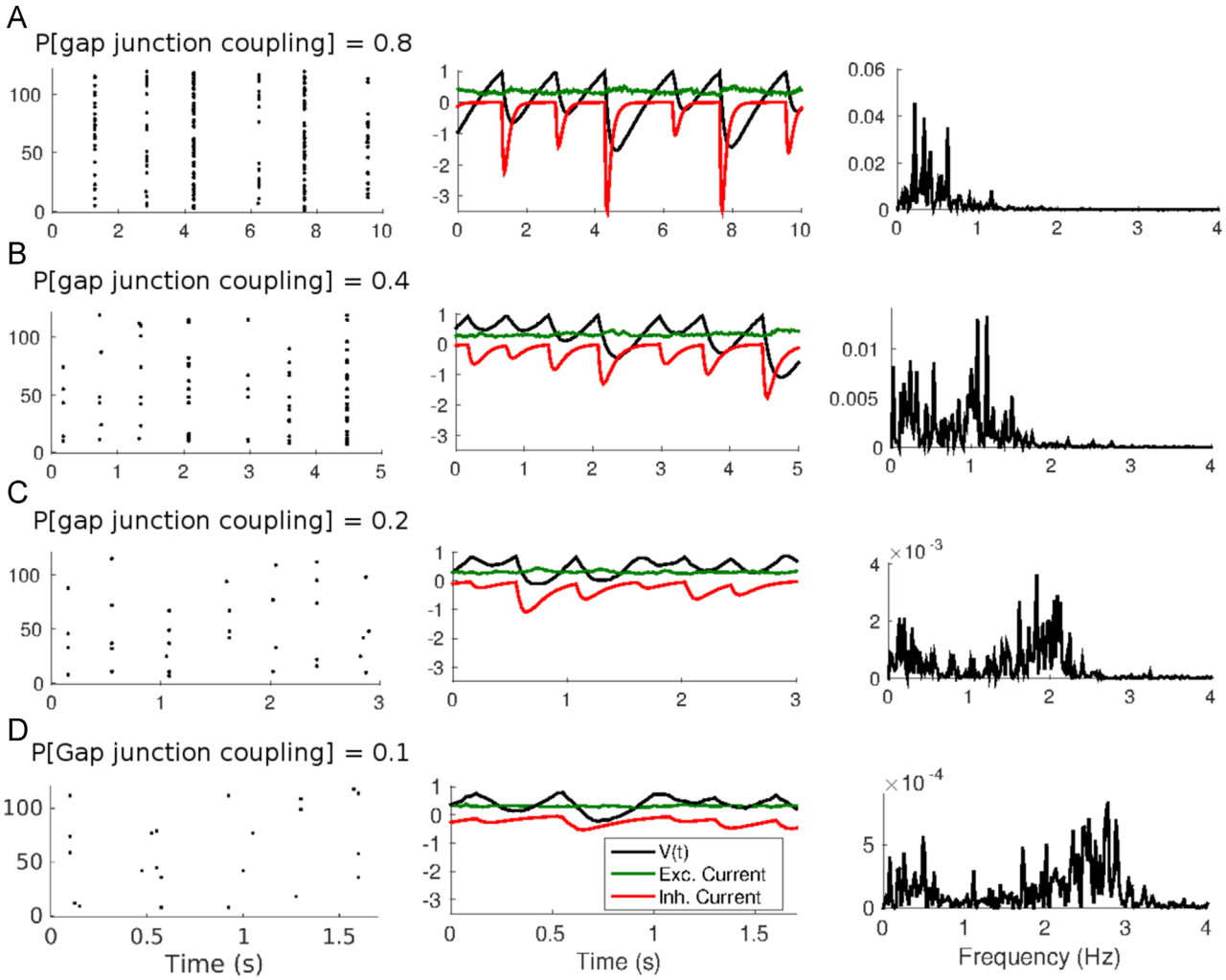

Fig. 6 – Effect of gap junction pruning on network oscillations. Spike rasters (*left*), membrane potential of a representative network neuron (*middle*), and power spectrum of the network's local field potential (*right*) are shown as gap junctions are pruned. Gap junction pruning is simulated by reducing the probability of gap junction coupling within the network; results are shown for gap junction coupling probabilities of (A) 0.8, (B) 0.4, (C) 0.2, (D) 0.1. As gap junctions are pruned from a coupling probability of 1 to 0.1, the network oscillation frequency increases from ~0.4 to ~3 Hz, while oscillatory power appears to decrease (note crispness of oscillations in spike rasters and peak sizes in power spectra). P[inhibitory synaptic coupling]=0.5 in all cases.

neonatal frequency of ~0.4 Hz), while a coupling probability of ~0.4 entails a further rise in the oscillation frequency to ~1.2 Hz, and coupling probabilities of 0.2 and 0.1 yield further increases in the network oscillation frequency to ~2 Hz and ~3 Hz, respectively. Furthermore, the crispness of the network oscillation declines as gap junction coupling is reduced, as evident from the plots of sample neurons from networks with a coupling probability of 1 (Fig. 2C) down to a coupling probability of 0.1 (Fig. 6); the subthreshold membrane potential oscillations, as well as the oscillations in the net synaptic inhibitory current received by a neuron, decrease in magnitude and sharpness with reductions in gap junction coupling probability. The reduction in the amplitude of the network oscillation as gap junctions are pruned is quantified in Fig. 7 – it shows that the integrated power in the 0.1–4 Hz range of the power spectrum of the network LFP declines as the frequency of the network oscillation increases (or, alternatively, as the gap junction coupling probability of the network is reduced).

How does progressive elimination of gap junctions lead to a rise in the global oscillation frequency while causing a decline in the amplitude of the network oscillation? With extensive (all-to-all) gap junction coupling, the direct electrical interconnectedness of the entire network yields global synchrony – when one neuron fires, gap junction coupling leads to all or most neurons firing simultaneously, which in turn causes delivery of synchronous, potent, and nearly identical synaptic inhibition to all network neurons. Hence, all network cells are suppressed for a prolonged period of time that is determined by the temporal dynamics of inhibitory synapses (several seconds), and the next network-wide synchronous burst occurs once the global inhibitory drive relents. With gap junction coupling reduced slightly, a single neuron reaching spike threshold is unable to drag the membrane potential of *all* neurons to threshold – rather, a single neuron reaching spike threshold causes a subset of network cells to follow suit, yielding a synchronous burst of spikes from a subset of

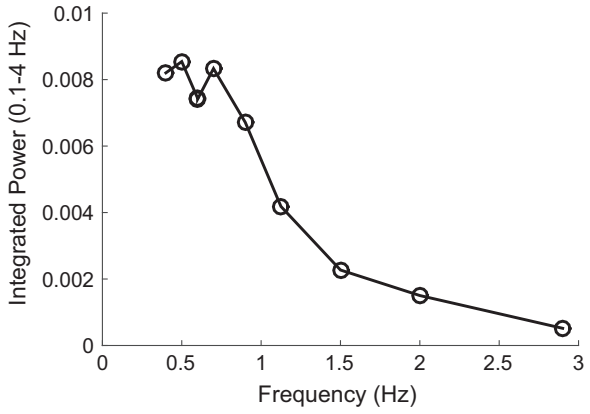

Fig. 7 – Dependence of network oscillatory power on oscillation frequency as gap junctions are pruned. The figure shows integrated power in the 0.1–4 Hz range of the network local field potential's power spectrum as a function of the oscillation frequency of the network. Each peak network oscillation frequency corresponds to a gap junction coupling probability as follows (frequency, probability): (0.4,1); (0.45,0.9); (0.6,0.8); (0.6,0.7); (0.7,0.6); (0.9,0.5); (1.15,0.4); (1.5,0.3); (2,0.2); (2.8,0.1). As gap junctions are pruned and network oscillation frequency rises, the amplitude of the network oscillation decreases. P [inhibitory synaptic coupling]=0.5 in all cases.

network neurons. Since only a subset of network neurons participate in the burst, the synaptic inhibition delivered to the entire network is not homogeneous – some cells receive more and some receive less inhibition, and a neuron that receives less inhibition is able to spike sooner, and (due to gap junctions) this neuron reaching spike threshold drags another subset of susceptible neurons to threshold, yielding the next synchronous spike burst. As a consequence of the nonhomogeneous synaptic inhibition produced by the initial spike burst, the next synchronous spike burst occurs after a shorter period of time than in the case of homogeneous inhibition when coupling is all-to-all, resulting in a higher network oscillation frequency. Moreover, since each spike burst results in reduced amplitude and less homogeneous network-wide inhibition, the magnitude of the network oscillation declines. As gap junctions are further pruned, this effect becomes progressively more prominent – the number of neurons participating in a spike burst declines, and each spike burst delivers a lower amount of less homogeneous inhibition to the network, allowing the next spike burst to occur with a diminishing interburst period and a declining network oscillation amplitude. Thus, progressive gap junction pruning causes the global oscillation frequency to rise (from 0.4 to 3 Hz) and the amplitude of the network oscillation to decrease; once gap junctions are eliminated entirely, the network oscillation vanishes.

2.3. *Excitation and gap junctions*

In our model, we include chemical synapses of only the inhibitory variety; however, in the neonatal rat LC, there are both inhibitory chemical synapses (mediated via α_2 adrenergic receptors) as well as excitatory chemical synapses (mediated via α_1 adrenergic receptors), with excitatory synapses vanishing during the P8–P21 developmental period (Williams and Marshall, 1987). While our results indicate that inhibitory synapses (along with gap junctions) are sufficient to account for LC physiology through early development, it is possible that a changing level of excitation within the rat LC during the P8–P21 period plays a role in LC dynamics. In this section, we therefore examine the relationship between excitation within our model and the ability of electrical coupling to generate network synchrony and oscillations.

In Fig. 8, we show spike rasters from our network in which the gap junction coupling probability is fixed at 0.5 but the amplitude of the noisy excitatory driving current delivered to neurons within the network is varied (cases in which the excitatory driving current has 1, 2, 3, 4, and 5 times its standard amplitude are shown). At the standard excitatory current amplitude, oscillations are fairly crisp and the network oscillation frequency is ~0.9 Hz. As the excitatory current amplitude is increased from its standard value to five-fold its standard value, the network oscillation frequency rises slightly (up to a maximum value of ~1.5 Hz at four-fold the standard value of the excitatory current amplitude), while the sharpness of the global network oscillation diminishes (increasing the amplitude of excitation causes network behavior to exhibit periods synchrony and oscillations interspersed with periods of asynchrony, with the relative length of asynchronous periods increasing with the level of excitation). At five-fold the standard value of the excitatory current amplitude, excitation overwhelms the ability of electrical coupling to synchronize cells, and the tendency of the network to globally oscillate vanishes. In the bottom right panel of Fig. 8 we show the oscillatory power of the network (the integrated power in the 0.1–4 Hz range of the power spectrum of the network LFP) as a function of the amplitude of the strength of the excitatory drive (labeled on the abscissa as the factor multiplying the standard excitatory current amplitude) – as the strength of the excitatory drive is increased, the global oscillatory tendency of the network decreases monotonically.

Thus, increasing excitation within the network leads to a decline in synchrony and oscillations. However, we find that it is not the level of excitation per se that determines the strength of the network oscillation; rather, it is the *ratio* of excitation to gap junction coupling (or strength) within the network that determines the strength of oscillations. In the left and middle panels of Fig. 9, we show spike rasters from the network in which the excitatory drive is set to four- and five-fold its standard amplitude, but with the probability of gap junction coupling within the network increased (from 0.5) to 0.65 and 0.75, respectively, in the two cases. With more widespread gap junction coupling, the network oscillation appears to remain crisp and relatively large in magnitude despite the increased level of excitation, while the frequency of the network oscillation changes little (compare with top left panel of Fig. 8). In the right panel of Fig. 9, we take a gap junction coupling probability of 0.5 with the standard excitatory driving current to be a reference case, and we compute the oscillatory power of the network in the reference case as the integrated power in the 0.1–4 Hz range of the power spectrum of the network LFP. As we increase the strength of the excitatory drive (the abscissa shows the factor by

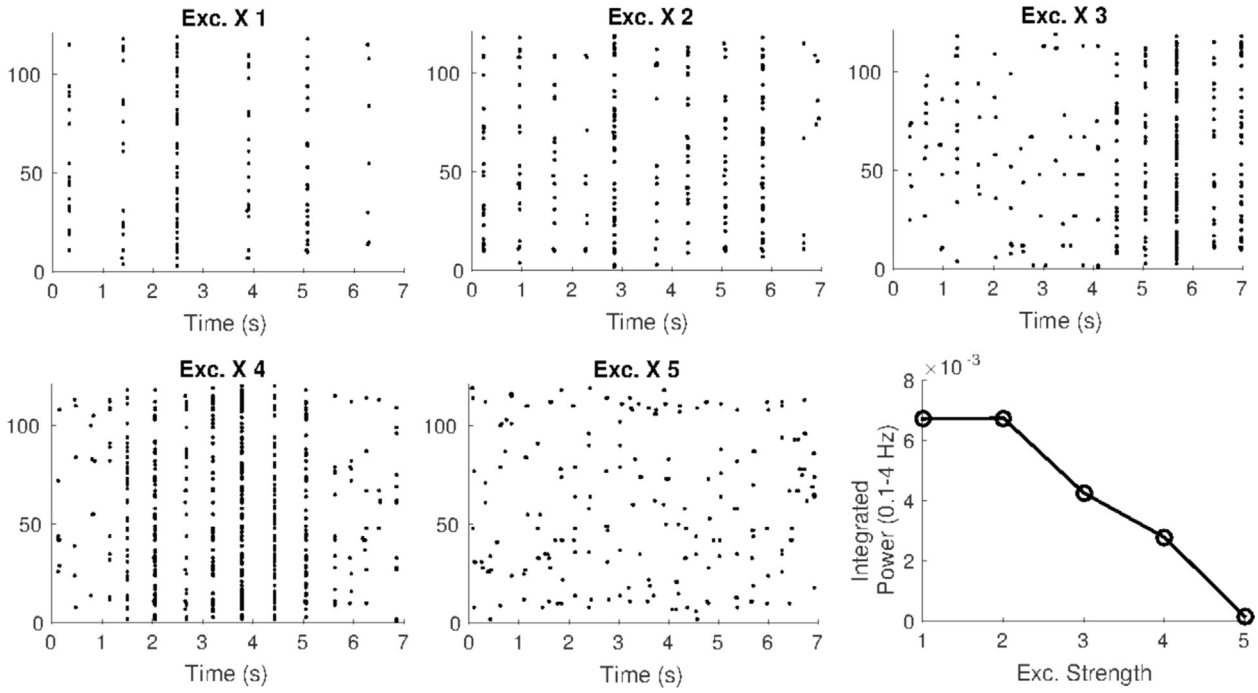

Fig. 8 – Dependence of network oscillations on the amplitude of the noisy excitatory driving current delivered to network neurons. The probability of gap junction coupling is fixed at 0.5, corresponding to an oscillation frequency of ~0.9 Hz with standard parameters (*top left panel*). As the amplitude of the excitatory driving current is increased, the oscillation frequency of the network increases slightly (up to ~1.5 Hz) while the oscillatory tendency of the network decreases and disappears for high levels of excitation (note crispness of oscillations in spike rasters and the integrated power in the 0.1–4 Hz range of the network local field potential's power spectrum for varying levels of excitation). P[inhibitory synaptic coupling]=0.5 in all cases.

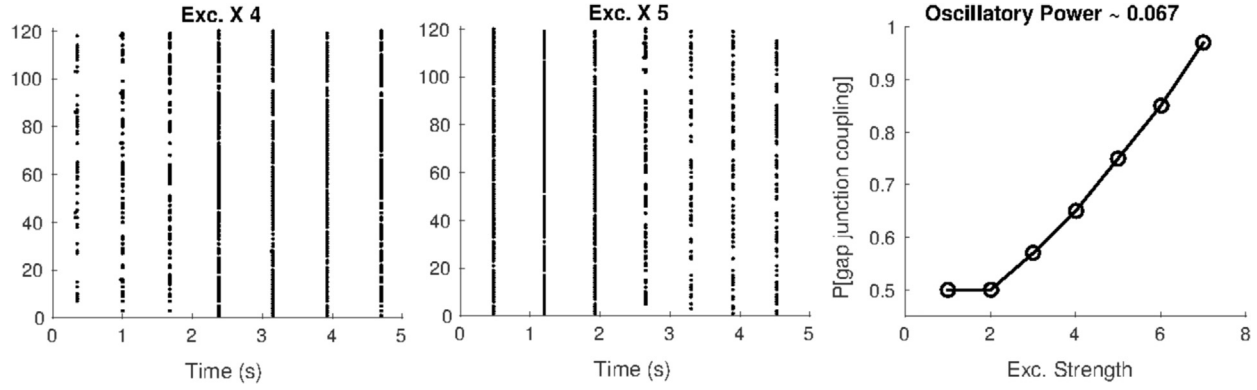

Fig. 9 – Gap junction coupling can be increased to compensate for increased excitation delivered to the network in order to maintain the network's oscillatory power, relative to a gap junction coupling probability of 0.5 (oscillatory frequency of ~0.9 Hz) with standard parameters (i.e., normal excitation amplitude). Integrated power of the network local field potential's power spectrum in the case of 0.5 gap junction coupling probability and normal excitatory amplitude is 0.0067. *Left:* **Spike raster when the excitatory amplitude is multiplied by 4 with the probability of gap junction coupling increased to 0.65 (integrated power=0.0066).** *Middle:* **Spike raster when the excitatory amplitude is multiplied by 5 with the probability of gap junction coupling increased to 0.75 (integrated power=0.0067).** *Right:* **Gap junction coupling probability required to maintain an oscillatory power of ~0.0067 for varying levels of the amplitude of excitation. In all cases, the network oscillation frequency remains between 0.9 and 1.5 Hz. P[inhibitory synaptic coupling]=0.5 in all cases.**

which the standard excitatory strength is multiplied) we plot on the ordinate the probability of gap junction coupling required to maintain the same oscillatory power as in the reference case. Fig. 9 indicates that as the level of excitation within the network is increased, the prevalence of electrical coupling within the network must rise in order to maintain the same network oscillation strength. In other words, increases in excitation can be compensated for by corresponding increases in gap junction coupling to maintain the network in the same oscillatory state. This result is

consistent with those of Alvarez et al. (2002), in which the authors construct a model of two neurons that are coupled by gap junctions and each of which receives an external excitatory driving current, and showed that strong gap junctions can synchronize the two neurons for high or low levels of excitation, while weak electrical coupling can synchronize the two neurons when firing rates are low but not when firing rates are high.

Within the rat LC, excitatory α_1 receptor-mediated excitatory synapses dwindle and disappear during the P8–P21 developmental period (Williams and Marshall, 1987), presumably leading to a declining level of reverberant excitation within the LC network during this period. There is also progressive gap junction pruning within this period, leading to a rise in oscillation frequency as well as a decrease in the amplitude of the global oscillation. Within the rat LC, therefore, the function of diminishing excitation within the P8–P21 period may be to allow for a less precipitous drop in network oscillatory strength as gap junctions are successively eliminated while still allowing an increase in the network oscillation frequency (due to gap junction pruning).

3. Discussion

In this work, we construct a biophysical model of the neonatal rat LC and model the changing physiology of the rat LC through early development (the P8–P21 period). Our neonatal LC model contains slow synaptic inhibition as well as extensive slow gap junction coupling, and we show that these features are sufficient to produce the experimentally observed low-frequency synchronized oscillations in the neonatal rat LC (Christie, 1997). We show that random gap junction pruning within our model is able to account for the evolving physiology of the rat LC from P8 to P21 – namely, the increase in network oscillation frequency up to ~3 Hz and the decrease in the amplitude of the network-wide oscillation (with subsequent disappearance of global synchrony) (Christie, 1997). Furthermore, we show that, for a given level of gap junction coupling, the time course of synaptic inhibition determines the frequency of the network oscillation while the strength of the network oscillation decreases as the level of excitation within the network is increased.

3.1. *Model parameters*

We make several simplifications in our model in service of computational efficiency, though our model parameters are chosen to remain consistent with available experimental data (see *Experimental procedures* for details). Rather than explicitly rendering a separate dendritic compartment to simulate the dendro-dendritic gap junctions found in the neonatal rat LC, we include a single compartment and replicate the slow time course of dendro-dendritic gap junctions by sending a time-averaged electrical potential from one neuron to a recipient neuron through the gap junction coupling term; we find that this scheme for emulating dendritic electrical coupling yields similar results to explicitly modeling a separate dendritic compartment. Moreover, we use an integrate-and-fire neuron model rather than a spiking neuron model to simulate individual LC neurons, which means that action potential transmission through gap junctions is neglected (since spikes are not explicitly rendered in an integrate-and-fire model). However, in the neonatal rat, LC action potentials (which occur over ~2 ms) are too fast to be transmitted through slow dendritic gap junctions (Christie, 1997), which justifies neglecting spike transmission through gap junctions in our model. Finally, we do not incorporate the Ca and Ca-dependent K currents found in neonatal LC neurons within our model, since experimental data suggest that synaptic mechanisms are sufficient to generate the post-activation inhibition observed in LC neurons (Ennis and Aston-Jones, 1986), and our purpose in this work is to investigate the changing oscillatory properties of the LC rather than the details of individual neuronal dynamics. Additionally, the physiological effect of intrinsic currents is likely to prevent an individual LC neuron from emitting several spikes in rapid succession, and in our model auto-inhibition (a neuron is able to synaptically inhibit itself Christie, 1997; Egan et al., 1983; Groves and Wilson, 1980; Ennis and Aston-Jones, 1986) produces this dynamical effect.

3.2. *Other models*

The mechanism of generating synchronized oscillations in our neonatal LC model (with all-to-all gap junction coupling) has some similar features to the interneuron gamma (ING) mechanism of synchronization via inhibitory interneurons, in which a chance event in which inhibitory cells spike together leads to network-wide synchronized inhibition, delaying network spiking until the inhibition decays and yielding a more synchronous burst of spikes once the inhibition has subsided, leading to progressive synchronization. In the ING mechanism, the period of the oscillation is determined by the firing rate of the inhibitory cells, and the ING mechanism is effective at yielding synchronized oscillations only when the decay time of synaptic inhibition matches the period of the oscillation (Tiesinga and Sejnowski, 2009). In our model, because of gap junction coupling, the inhibitory cells synchronize even without inhibition (i.e., if the amplitude of synaptic inhibition is set to 0) and in the presence of strong inhibition the decay time of synaptic inhibition serves to set the period of the oscillation by quieting all network cells for a characteristic period of time after each synchronous spike burst. Thus, the presence of gap junctions in our model allows for synchronized oscillations over a much wider range of frequencies (with the time course of inhibition determining the oscillation period) than in the ING mechanism.

The relationship between electrical coupling and neuronal synchrony has been examined in some detail by other investigators. In Dodla and Wilson (2013) and Chow and Kopell (2000), the authors carry out mathematical analyses of a pair of electrically coupled neurons and study the effects of gap junction coupling on the existence and stability of phase-locked states within the two-neuron system. In Alvarez et al. (2002) the authors construct a model of two LC neurons coupled via dendritic gap junctions and driven by external currents, and the investigators show computationally that strong gap junctions can synchronize the two neurons for all firing frequencies, while weak electrical

coupling can synchronize the two neurons when firing rates are low but not for high firing rates; this result is borne out in our larger LC model, since in our model the ability of gap junctions to synchronize the network depends on the ratio of the strength of excitation to gap junction efficacy (too high a ratio hinders the ability of gap junctions to synchronize the network – see Section 2.3). Other studies have examined synchronization in networks of electrically coupled neurons (Latorre et al., 2013; Medvedev and Zhuravytska, 2012a, 2012b) and the role of LC gap junctions in behavioral tasks (Usher et al., 1999).

The addition of synaptic inhibition, however, can yield different dynamical behavior. Several studies (Lewis and Rinzel, 2003; Lewis, 2003; Bem and Rinzel, 2004; Nomura et al., 2003) mathematically analyze a pair of neurons coupled via gap junctions and inhibitory chemical synapses, showing that a combination of chemical and electrical coupling can yield both synchronous and antisynchronous stable states. These results provide a small-scale analog to the behavior of our larger LC model within the context of gap junction pruning – as gap junctions are pruned within our model, the network exhibits stable steady-state behavior consisting of oscillating out-of-phase clusters of LC neurons. Other studies have examined the properties of networks of neurons connected via gap junctions and synaptic inhibition (Juan Gao and Holmes, 2007; Guo et al., 2012; Kopell and Ermentrout, 2004; Skinner et al., 1999; Traub et al., 2001; Gutierrez et al., 2013). In Guo et al. (2012) and Kopell and Ermentrout (2004) the authors find that gap junctions are more effective at generating tight synchrony than synaptic inhibition, which is consistent with the behavior of our model (compare Fig. 2A and B), and in Traub et al. (2001) the investigators show that even modest electrical coupling can stabilize global gamma oscillations in networks of inhibitory interneurons – similar behavior is seen in our model, since both gap junctions and synaptic inhibition are needed in our network in order for synchronized oscillations to emerge (see Fig. 2).

To our knowledge, however, the unique dynamics of the evolving infant LC network (the rising network oscillation frequency, decreasing global oscillation amplitude, the presence of slow dendro-dendritic gap junctions with slow synaptic inhibition, and gap junction pruning) have not received detailed examination in prior work. In this study, we investigate the specific architecture and physiology of the infant LC network and the changes in the dynamical behavior of the infant LC through the early developmental period. We propose mechanisms for evolving LC dynamics, and we examine the dependence of LC behavior on network parameters in a biophysically realistic infant LC model.

As discussed in the *Introduction*, the LC appears to play a central role in modifying sleep–wake switching behavior through early development. The LC interacts with mutually inhibitory sleep-active and wake active populations and causes the wake bout distribution to transform from exponential to power law-like during the P8–P21 period. We are currently developing a model of mutually inhibitory sleep-active and wake-active populations (Patel and Joshi, 2014), and in future work, we will couple our model of mutually inhibitory sleep-active and wake-active populations with the LC model presented in this paper in order to assess the physiological mechanisms by which the LC influences the infant sleep–wake circuit during the P8–P21 period.

4. Experimental procedures

Our rat LC model consists of 120 integrate-and-fire neurons coupled via weak dendritic gap junctions and inhibitory α_2 receptors (since spikes are too fast to be transmitted via slow dendritic gap junctions, explicit modeling of the spiking mechanism is unnecessary). For the standard neonatal LC model, gap junction coupling is random with a coupling probability of 1 between any two neurons, and inhibitory synaptic coupling is random with a probability of 0.5 of a synapse between any one neuron and another. Additionally, neurons are self-coupled (each neuron is capable of inhibiting itself, as observed experimentally) (Christie, 1997; Egan et al., 1983; Groves and Wilson, 1980; Ennis and Aston-Jones, 1986). In simulations where the probability of gap junction coupling is varied, this is achieved by mimicking the physiological process of gap junction pruning. Whether neuron i is electrically coupled to neuron j is determined by a randomly generated number between 0 and 1 – if this random number is less than the gap junction coupling probability of the network, neurons i and j are coupled, otherwise they are not. Reductions in the gap junction coupling probability of the network are effected by decreasing the gap junction coupling probability of the network while keeping the same random seed for the simulation; this causes the same random numbers to be generated, with the only difference being a decrease in the threshold required for two neurons to lack electrical coupling. Once the (fixed) random number generated for neurons i and j is greater than this threshold, the gap junction between neurons i and j is eliminated. Hence, this scheme corresponds to reductions in the gap junction probability of the network yielding progressive elimination of gap junctions within the network while maintaining the remaining network architecture. We chose this method in order to simulate the biological process of gap junction pruning; however, we note that this pruning process is not necessary to obtain the results in this paper – similar results are seen if, when going from a gap junction coupling probability of $p1$ to $p2$ ($<p1$), gap junction coupling is generated anew with probability $p2$ rather than undergoing the pruning process described above.

The membrane potential of neuron j within the LC model is governed by integrate-and-fire dynamics:

$$\frac{dv_j}{dt} = -g_L(v_j - E_L) - g_j(t)(v_j - E_i) - \sum_k g_c(v_j - \hat{v}_k) + i_j(t), \quad (1)$$

$$\hat{v}_k(t) = \frac{1}{50}\int_{t-50}^{t} v_k(s)\, ds, \quad (2)$$

$$v_j(t) \geq 1 \Longrightarrow v_j(t) = 0. \quad (3)$$

The model is a modification of a reduced dimensional integrate-and-fire model of a cortical cell (Tao et al., 2004). $v_j(t)$ is the nondimensional membrane potential, $E_L = 0$ is the nondimensional leak potential, and $E_i = -2.67$ is the nondimensional reversal potential for synaptic inhibition

(calculated using the reversal potential of -104 mV of K^+ channels opened via α_2 receptor-mediated synaptic inhibition in LC neurons) (Egan et al., 1983). $g_L = 0.05\ \mathrm{ms}^{-1}$ is the leak conductance, and $g_j(t)$ is the synaptic inhibitory conductance. A spike is recorded for neuron j and $v_j(t)$ is reset to the resting potential E_L when $v_j(t)$ crosses the spiking threshold of 1.

A presynaptic spike leads to a change in $g_j(t)$ modeled as an alpha function with a long time course (Egan et al., 1983); if there are a total of n_j presynaptic spikes to neuron j with the rth spike occurring at time t_j^r, then the inhibitory conductance of neuron j is given by

$$g_j(t) = \sum_{r=1}^{n_j} g_j^r(t) \quad \text{where} \tag{4}$$

$$g_j^r(t) = 0\left(t < t_j^r\right), \quad g_j^r(t) = A\frac{t - t_j^r}{\tau} e^{-(t-t_j^r)/\tau}\left(t \geq t_j^r\right). \tag{5}$$

A describes the amplitude of synaptic inhibition, with a standard value of $A = 0.3$. In simulations where the strength of synaptic inhibition is multiplied by a factor h, this is achieved by multiplying A by h. The standard value for the time course of synaptic inhibition is given by $\tau = 100$ ms. In simulations where the time course of synaptic inhibition is varied, τ is modified.

The third term in the membrane potential equation represents gap junction coupling, with the sum taken over all neurons electrically coupled to neuron j. $g_c = 0.045\ \mathrm{ms}^{-1}$ is the gap junction conductance, which is set at a value ~ten-fold larger than the conductance for a neonatal rat LC gap junction calculated using the strength of gap junction coupling between LC neurons observed experimentally. In the rat LC, a ~100 mV potential change in one neuron leads to a ~2 mV change in a gap junction coupled neuron (Christie et al., 1989; Travagli et al., 1995).

The connection between physiological gap junction strength and g_c in our model is derived as follows. Consider an integrate-and-fire model for a neuron electrically coupled to a single other neuron whose membrane potential is fixed at a value α; this corresponds to equation 1) with $g_j(t) = 0$, $k = 1$, $\hat{v}_1 = \alpha$, and $i_j(t) = 0$. Suppose $v(0) = E_L = 0$. Neglecting spiking, this is simply a first order linear equation that we can solve explicitly for $v_j(t)$. The $\lim_{t\to\infty} v_j(t)$ tells us the steady state value that $v_j(t)$ will approach when gap junction coupled to a neuron with a constant membrane potential given by α. Since in the actual rat LC, a 100 mV change in a neuron leads to a 2 mV change in a gap junction-connected neuron, or in other words a change in the membrane potential of a neuron causes a 50-fold smaller change in the membrane potential of a gap junction-connected neuron, we set $\lim_{t\to\infty} v_j(t) = \alpha/50$ and we solve for the gap junction conductance g_c required for the steady state value of $v_j(t)$ to be 1/50 th that of α, and we obtain $g_c = \sim 0.001$. Hence, if $v_j(t)$ starts at rest and is gap junction coupled to a neuron set at membrane potential α, then a gap junction conductance of $g_c = \sim 0.001$ will cause $v_j(t)$ to change by 1/50 th of α. Gap junction conductance is set at a larger value in our model ($g_c = 0.045$) in order to prevent a precipitous drop in network oscillatory power as gap junctions are pruned – since our network is scaled down (120 neurons versus 1500 in the actual rat LC), gap junction pruning within our network would cause a more rapid decline in the effectiveness of electrical coupling than would be observed in the rat LC if we did not increase the strength of individual gap junctions. For our neonatal rat LC model (i.e., the model presented in this paper in the case that gap junction coupling is all-to-all), a ten-fold decrease in the gap junction conductance yields similar results to those presented.

In our model, we average the input membrane potential of a neuron k electrically coupled to neuron j over the past 50 ms in order to mimic the slow time scale of dendro-dendritic gap junctions within the LC, and the lack of explicit spiking in the integrate-and-fire model automatically simulates the fact that spikes are too fast to be transmitted via slow dendritic gap junctions (Christie et al., 1989). We find that this scheme for emulating dendro-dendritic gap junctions yields similar behavior to explicitly rendering a separate dendritic compartment.

$i_j(t)$ is a noisy excitatory current, modeled as a Poisson process of spikes arriving from outside the LC. Incoming spikes arrive at a Poisson rate of B spikes/ms, and each incoming spike causes a jump in $i_j(t)$ of C ms^{-1}, with exponential decay governed by a 50 ms time constant, in accordance with the experimentally observed dynamics of outside excitatory inputs impinging upon infant rat LC neurons (Cherubini and North, 1988). Standard values for B and C are given by $B = 1$ and $C = 0.0015$. In simulations where the strength of excitation is multiplied by a factor h, this is achieved by multiplying both the values of B and C by $\sqrt{h}$.

We find that the results presented in this paper are robust over an ensemble of randomly connected networks (the specific randomly generated architecture employed in this paper is not needed to obtain the results shown). In order to obtain the results presented in this paper, the parameters must be chosen such that inhibition within the network is strong (relative to excitation), that the time scale of synaptic inhibition is long enough to ensure that oscillations have a low frequency (in the presence of extensive gap junction coupling), and that electrical coupling (when extensive) must be sufficient to generate network-wide synchrony. Furthermore, the probability of inhibitory coupling can be varied from ~0.1 to 1.0 without changing qualitative network behavior, though inhibition must be strengthened as the probability of inhibitory coupling is lowered (coupling must simply be sufficient to yield a potent inhibitory drive that pervades the network).

Each simulation is run for a total time of 60 s using the explicit Euler method with a time step of 0.1 ms. The local field potential of the network is computed as the average membrane potential of all neurons within the network. The power spectrum of the local field potential is computed over 55 s (from 5 s to 60 s) in order to allow the initial transient behavior of the network to decay.

Acknowledgments

We would like to thank the College of William and Mary, Department of Mathematics and the California State University, San Marcos, Department of Mathematics.

REFERENCES

Alvarez, V., Chow, C., van Bockstaele, E., Williams, J., 2002. Frequency-dependent synchrony in locus ceruleus: role of electrotonic coupling. Proc. Natl. Acad. Sci. USA 99 (6), 4032–4036.

Aston-Jones, G., Bloom, F.E., 1981. Activity of norepinephrine-containing locus coeruleus neurons in behaving rats anticipates fluctuations in the sleep-waking cycle. J. Neurosci. 1 (8), 876–886.

Bem, T., Rinzel, J., 2004. Short duty cycle destabilizes a half-center oscillator, but gap junctions can restabilize the anti-phase pattern. J. Neurophysiol. 91 (2), 693–703.

Berridge, C., Schmeichel, B., Espana, R., 2012. Noradrenergic modulation of wakefulness/arousal. Sleep Med. Rev. 16, 187–197.

Blumberg, M.S., Seelke, A.M.H., Lowen, S.B., Karlsson, K., 2005. Dynamics of sleep–wake cyclicity in developing rats. Proc. Natl. Acad. Sci. USA 102 (41), 14860.

Cherubini, E., North, R., 1988. Synaptic potentials in locus coeruleus neurons. J. Physiol. 406, 431–442.

Chow, C., Kopell, N., 2000. Dynamics of spiking neurons with electrical coupling. Neural Comput. 12 (7), 1643–1678.

Christie, M., 1997. Generators of synchronous activity of the locus coeruleus during development. Semin. Cell Dev. Biol. 8 (1), 29–34.

Christie, M., Jelinek, H., 1993. Dye-coupling among neurons of rat locus coeruleus during postnatal development. Neuroscience 56, 129–137.

Christie, M., Williams, J., North, R., 1989. Electrical coupling synchronizes subthreshold activity in locus coeruleus neurons in vitro from neonatal rats. J. Neurosci. 9, 3584–3589.

Coyle, J., Molliver, M., 1977. Major innervation of newborn rat cortex by monoaminergic neurons. Science 196, 444–447.

Dodla, R., Wilson, C., 2013. Effect of sharp jumps at the edges of phase response curves on synchronization of electrically coupled neuronal oscillators. PLoS One 8, 1–16.

Egan, T., Henderson, G., North, R., Williams, J., 1983. Noradrenaline-mediated synaptic inhibition in rat locus coeruleus neurones. J. Physiol. 345, 477–488.

Ennis, M., Aston-Jones, G., 1986. Evidence for self- and neighbor-mediated postactivation inhibition of locus coeruleus neurons. Brain Res. 374 (2), 299–305.

Gall, Andrew, Joshi, Badal, Best, Janet, Florang, Virginia R., Doorn, Jonathan A., Blumberg, Mark, 2009. Developmental emergence of power-law wake behavior depends upon the functional integrity of the locus coeruleus. Sleep 32 (7), 920–926.

Juan Gao, Holmes, Philip, 2007. On the dynamics of electrically-coupled neurons with inhibitory synapses. J. Comput. Neurosci. 22 (1), 39–61.

Groves, P., Wilson, C., 1980. Fine structure of rat locus coeruleus. J. Comp. Neurol. 193, 841–852.

Guo, D., Wang, Q., Perc, M., 2012. Complex synchronous behavior in interneuronal networks with delayed inhibitory and fast electrical synapses. Phys. Rev. E 85, 061905–061913.

Gutierrez, G., OĹeary, T., Marder, E., 2013. Multiple mechanisms switch an electrically coupled, synaptically inhibited neuron between competing rhythmic oscillators. Neuron 77 (5), 845–858.

Halász, P., Terzano, M., Parrino, L., Bódizs, R., 2004. The nature of arousal in sleep. J. Sleep Res. 13 (1), 1–23.

Ishimatsu, M., Williams, J., 1996. Synchronous activity in locus coeruleus results from dendritic interactions in pericoerulear regions. J. Neurosci. 16, 5196–5204.

Karlsson, K., Kreider, J.C., Blumberg, M.S., 2004. Hypothalamic contribution to sleep–wake cycle development. Neuroscience 123 (2), 575–582.

Karlsson, K.Æ, Gall, A.J., Mohns, E.J., Seelke, A.M.H., Blumberg, M. S., 2005. The neural substrates of infant sleep in rats. PLoS Biol. 3 (5), e143.

Kleitman, N., Engelmann, T.G., 1953. Sleep characteristics of infants. J. Appl. Physiol. 6 (5), 269–282.

Kopell, N., Ermentrout, B., 2004. Chemical and electrical synapses perform complementary roles in the synchronization of interneuronal networks, Proc. Natl. Acad. Sci. USA 101 (43) (2004), 15482–15487.

Latorre, R., Aguirre, C., Rabinovich, M., Varona, P., 2013. Transient dynamics and rhythm coordination of inferior olive spatio-temporal patterns. Front. Neural Circuits 7 (138), 1–18.

Lewis, T., Rinzel, J., 2003. Dynamics of spiking neurons connected by both inhibitory and electrical coupling. J. Comput. Neurosci. 14 (3), 283–309.

Lewis, Timothy J., 2003. Phase-locking in electrically coupled non-leaky integrate-and-fire neurons, discrete and continuous dynamical systems. In: Proceedings of 4th International Conference on Dynamical Systems and Differential Equations, Supplementary volume, 2003, pp. 554–562.

Lo, C.C., Chou, T., Penzel, T., Scammell, T.E., Strecker, R.E., Stanley, H.E., Ivanov, P.C., 2004. Common scale-invariant patterns of sleep–wake transitions across mammalian species. Proc. Natl. Acad. Sci. USA 101 (50), 17545.

Lo, C.C., Nunes Amaral, L.A., Havlin, S., Ivanov, P.C., Penzel, T., Peter, J.H., Stanley, H.E., 2002. Dynamics of sleep–wake transitions during sleep. Europhys. Lett. (EPL) 57, 625.

Medvedev, G., Zhuravytska, S., 2012a. The geometry of spontaneous spiking in neuronal networks. J. Nonlinear Sci. 22 (5), 689–725.

Medvedev, G.S., Zhuravytska, S., 2012b. Shaping bursting by electrical coupling and noise, Biol. Cybern. 106 (2012), 67–88.

Nomura, M., Fukai, T., Aoyagi, T., 2003. Synchrony of fast-spiking interneurons interconnected by gabaergic and electrical synapses. Neural Comput. 15 (9), 2179–2198.

Patel, M., Joshi, B., 2014. Switching mechanisms and bout times in a pair of reciprocally inhibitory neurons. J. Comput. Neurosci. 36, 177–191.

Saper, C., Chou, T., Scammell, T., 2001. The sleep switch: hypothalamic control of sleep and wakefulness. Trends Neurosci. 24 (12), 726–731.

Schwartz, J., Roth, T., 2008. Neurophysiology of sleep and wakefulness: basic science and clinical implications. Curr. Neuropharmacol. 6, 367–378.

Skinner, F., Zhang, L., Perez-Velazquez, J., Carlen, P., 1999. Bursting in inhibitory interneuronal networks: a role for gap-junctional coupling. J. Neurophysiol. 81, 1274–1283.

Takahashi, K., Kayama, Y., Lin, J., Sakai, K., 2010. Locus coeruleus neuronal activity during the sleep-waking cycle in mice. Neuroscience 169, 1115–1126.

Tao, L., Shelley, M., McLaughlin, D., Shapley, R., 2004. An egalitarian network model for the emergence of simple and complex cells in visual cortex. Proc. Natl. Acad. Sci. USA 101 (1) (2004), 366.

Tiesinga, P, Sejnowski, T., 2009. Cortical enlightenment: are attentional gamma oscillations driven by ING or PING. Neuron 63 (6), 727–732.

Traub, R., Kopell, N., Bibbig, A., Buhl, E., Lebeau, F., Whittington, M., 2001. Gap junctions between interneuron dendrites can enhance synchrony of gamma oscillations in distributed networks. J. Neurosci. 21, 9478–9486.

Travagli, R., Dunwiddie, T., Williams, J., 1995. Opioid inhibition in locus coeruleus. J. Neurophysiol. 74, 518–528.

Usher, M., Cohen, J., Servan-Schreiber, D., Rajkowski, J., Aston-Jones, G., 1999. The role of locus coeruleus in the regulation of cognitive performance. Science 283, 549–554.

Williams, J., Marshall, K., 1987. Membrane properties and adrenergic responses in locus coeruleus neurons of young rats. J. Neurosci. 7, 3787–3794.